First-principles study of boron speciation in calcite and aragonite

Etienne Balan, Fabio Pietrucci, Christel Gervais, Marc Blanchard, Jacques Schott, Jérome Gaillardet

First-principles study of boron speciation in calcite and aragonite

Revision 1

Etienne Balan[a,*], Fabio Pietrucci[a], Christel Gervais[b], Marc Blanchard[a], Jacques Schott[c], Jérome Gaillardet[d]

[a]Sorbonne Universités - Institut de Minéralogie, de Physique des Matériaux et de Cosmochimie (IMPMC), UPMC Université Paris 06, UMR CNRS 7590, UMR IRD 206, MNHN, 4 place Jussieu, 75252 Paris cedex 05, France

[b]Sorbonne Universités - Laboratoire de Chimie de la Matière Condensée de Paris (LCMCP), UPMC Université Paris 06, UMR CNRS 7574, 4 place Jussieu, 75252 Paris cedex 05, France

[c]Géosciences Environnement Toulouse, Observatoire Midi-Pyrénées, CNRS-Université de Toulouse, 14, avenue Edouard Belin 31400 Toulouse, France

[d]Institut de Physique du Globe de Paris, Sorbonne Paris Cité, Université Paris Diderot, CNRS, F-75005 Paris, France, and Institut Universitaire de France.

[*]Corresponding author: Prof. Etienne Balan, Institut de Minéralogie, Physique des Matériaux et Cosmochimie, Case 115, 4 Place Jussieu, 75252 Paris Cedex 05. tel: 00.33.1.44.27.74.52 fax: 00.33.1.44.27.37.85 E-mail: Etienne.Balan@impmc.upmc.fr

Abstract

Despite the importance of boron as a proxy of past ocean pH, the crystal-chemical factors controlling its incorporation in the structure of calcium carbonates are still poorly understood. This is partly linked to an imperfect knowledge of the coordination, protonation state and local environment of boron species in these minerals. In the present study, we use first-principles quantum mechanical tools to model selected trigonal and tetragonal boron species in calcite and aragonite. The stable geometry of the models is obtained from standard energy minimization schemes or using a more advanced metadynamics exploration of their configurational space. The computation of ^{11}B NMR chemical shifts and quadrupolar coupling parameters enables a straightforward comparison of the models to existing experimental NMR data. The results show that B in calcium carbonates does occur as structural species substituted for CO_3^{2-} anions. The B speciation depends on the polymorph considered. In calcite, structural boron is present as partially deprotonated trigonal $BO_2(OH)^{2-}$ species coexisting with a fraction of substituted $B(OH)_4^-$ groups. In aragonite, the $B(OH)_4^-$ substitution for CO_3^{2-} anions is dominant. Different species, including entrapped $B(OH)_3$ molecules and substituted BO_3^{3-} groups also occur in biogenic samples. The diversity of B speciation reflects a diversity of B incorporation mechanisms and sheds light on previous studies confronting B isotopic composition determination with NMR observations. The mechanisms of boron incorporation in calcium carbonates are probably more complex than usually assumed in the literature using boron isotopes as a proxy of paleo-atmospheric CO_2 reconstructions. Although not invalidating the empirical paleo-pH proxy, these results call for a better understanding of the fundamental mechanisms of boron incorporation in carbonates.

1. INTRODUCTION

The isotopic composition of boron in biogenic calcite and aragonite has been proposed and successfully used as a proxy of the past ocean acidity, which in turn reflects past levels of atmospheric CO_2 concentrations (Vengosh et al. 1991; Hemming and Hanson 1992). A large number of studies have applied this idea to various biogenic carbonates, proposed paleo-CO_2 secular evolutions for the Earth's atmosphere and established the sensitivity of global climate to atmospheric CO_2 in the past (e.g., Spivack et al. 1993; Gaillardet and Allègre 1995; Sanyal et al. 1995; Palmer et al. 1998; Pearson and Palmer 1999; Lemarchand et al. 2002; Pagani et al. 2005; Pearson et al. 2009; Martinez-Boti et al. 2015). The use of boron isotopes as a paleo-pH meter is based on the large difference in $^{11}B/^{10}B$ ratio (27.2 ‰ in delta notation of isotopic abundances; Klochko et al. 2006) occurring between the major dissolved forms of boron, the trigonal boric acid ($B(OH)_3$, preferentially enriched in ^{11}B), and the tetragonal borate ion ($B(OH)_4^-$, preferentially enriched in ^{10}B), under thermodynamic equilibrium conditions (Zeebe 2005; Liu and Tossell 2005; Klochko et al. 2006; Rustad et al. 2010; Nir et al. 2015). As the relative proportion of these aqueous species is strongly pH-dependent in the range of expected seawater pH, mass balance considerations require that their isotopic composition is also pH-dependent. Assuming that among the two major B species present in seawater only the borate ion ($B(OH)_4^-$) is incorporated in the mineral structure during crystal growth and that no boron isotope fractionation occurs during uptake, the B isotopic composition in marine carbonate samples provides a straightforward record of the secular variations of seawater pH.

The assumption of sole $B(OH)_4^-$ incorporation is challenged by spectroscopic studies reporting various proportions of both trigonal and tetragonal B species

77 coexisting in calcite and aragonite samples. Both boron partitioning and speciation are
78 polymorph dependent, aragonite incorporating tetragonal boron more easily than
79 calcite (e.g. Sen et al. 1994; Branson et al. 2015; Mavromatis et al. 2015). Direct
80 determination of the boron coordination state can be achieved using ^{11}B solid-state
81 nuclear magnetic resonance (NMR) (Sen et al. 1994; Klochko et al. 2006; Rollion-Bard et
82 al. 2011; Mavromatis et al. 2015), electron energy loss spectroscopy (EELS) (Rollion-
83 Bard et al. 2001) and scanning transmission X-ray microscopy (STXM) (Branson et al.
84 2015). The observation of an often dominant contribution of trigonal B in calcite, and its
85 occurrence in aragonite, has been interpreted as reflecting a coordination change of
86 borate ions at the surface of growing crystals (Hemming et al. 1998; Klochko et al. 2009;
87 Branson et al. 2015). This interpretation is consistent with in-situ Atomic Force
88 Microscopy (AFM) observations of the morphology and dynamic of the surface of calcite
89 crystals growing from B-bearing solutions (Ruiz-Agudo et al. 2012). According to this
90 mechanism, the boron isotopic composition in the mineral phase still reflects that of the
91 borate ions in the solution. This explains the success of the boron-isotope proxy for
92 paleo-pH reconstitutions from mineral remains of extinct species. However, several
93 studies have suggested that a fraction of incorporated B could correspond to boric acid
94 molecules, directly scavenged from the solution (Xiao et al. 2008, Rollion-Bard et al.
95 2011, Noireaux et al. 2015). Consistently, higher than expected $^{11}B/^{10}B$ ratio have been
96 determined on inorganically precipitated and biogenic calcium carbonate samples.
97 Isotopic effects in biogenic carbonates have also been shown to depend upon the
98 calcifying species. Although local variations of pH at the calcification site can surely
99 contribute to the isotopic variability observed in biologically produced calcium
100 carbonates, inorganic precipitation experiments under well-constrained pH conditions

101 cannot be reconciled with models based on the exclusive incorporation of borate ions,
102 showing that the basis hypotheses of the paleo-pH theory are questionable.

103 Despite the importance of the boron-isotope pH proxy, the crystal-chemical
104 factors controlling boron incorporation in carbonates are still elusive. Several factors
105 impede a detailed understanding of its incorporation mechanisms. Differences between
106 the geometry of the stiff molecular tetragonal B anions and that of the trigonal
107 substitution sites can lead to substantial modifications of the medium-range structure
108 around the B species. Various electrostatic charge compensation mechanisms (e.g.
109 involving different protonation states, presence of vacancies, or incorporation of other
110 trace elements) can also affect the B environment, which significantly increases the
111 system complexity. These effects are difficult to determine from experiment because
112 spectroscopic methods usually provide information restricted to the well-defined first
113 coordination shell of boron. Complementary to experimental observations, theoretical
114 approaches can bring important constraints to discuss molecular-scale aspects of B
115 incorporation in calcium carbonates. Tossell (2005, 2006) has investigated the NMR
116 spectroscopic and the thermodynamic properties of boron species using molecular
117 modeling techniques. Although these studies mostly focused on B species in aqueous
118 solutions and did not treat explicitly the role of the crystalline matrix, they provided
119 quantitative relations between the geometry and protonation state of the boron
120 complexes and their distinctive NMR parameters. In the light of the experimental data of
121 Sen et al. (1994), Tossell (2005) suggested that the incorporation of trigonal B should
122 occur via a distorted, partially deprotonated group instead of more symmetric fully
123 protonated or deprotonated groups. Tossell (2006) and Klochko et al. (2009) also
124 suggested that chemically more complex species such as $B(OH)_2CO_3^-$ could account for
125 the experimental observations of Sen et al. (1994).

In this article, we use first-principles quantum mechanical calculations to determine the most favorable coordination states and geometry of boron species in calcite and aragonite and discuss related incorporation mechanisms. We theoretically determine the stable configuration of atomic-scale models of boron in calcium carbonates, using an approach similar to that previously developed to study sulfate incorporation in carbonates (Balan et al. 2014). The computation of the related NMR parameters (Pickard and Mauri 2001; Charpentier 2011; Bonhomme et al. 2012) then enables a straightforward comparison of the theoretical models to existing NMR experimental data. The results attest to the diversity of B speciation in synthetic and biogenic calcium carbonates; among which the substitution of partially protonated trigonal $BO_2(OH)^{2-}$ and fully protonated tetragonal $B(OH)_4^-$ groups for CO_3^{2-} anions are dominant.

2. METHODS

2.1 Structural optimization of models of boron-bearing calcium carbonates

First-principles quantum mechanical calculations provide the electronic density and total energy of a system made of nuclei and electrons by solving the corresponding Schrödinger equation. Many properties of a system (e.g. equilibrium structure, elastic constants, vibrational modes, ...) are in fact determined by the total energy and its variations. These methods are considered as highly predictive because their ingredients are not fitted on experimental data. All of them are however characterized by a trade-off between computation time and accuracy. In the past twenty years, methods based on

151 the density functional theory (DFT) have reached a level of accuracy high enough to
152 reproduce with an excellent agreement the static and dynamic properties of
153 geochemically relevant systems (see, e.g., Cygan and Kubicki 2001). The present
154 calculations were performed within the DFT framework, using periodic boundary
155 conditions and the generalized gradient approximation (GGA) to the exchange-
156 correlation functional as proposed by Perdew, Burke and Ernzerhof (PBE; Perdew et al.
157 1996). The ionic cores were described by ultra-soft pseudopotentials from the GBRV
158 library (Garrity et al. 2014); which means that only the electrons contributing to
159 chemical bonding are explicitly treated, while those occupying the core states are
160 considered to be unaffected by variations in the atom environment. The electronic
161 wave-functions and charge density were expanded using a finite basis sets of plane-
162 waves with 40 and 200 Ry cutoffs, respectively, corresponding to a convergence of the
163 total energy better than 1 mRy/atom.

164 Periodic models of boron-bearing calcium carbonates were built for the two
165 common $CaCO_3$ polymorphs: calcite ($R\bar{3}c$, 10 atoms per rhombohedral primitive cell)
166 and aragonite (*Pmcm*, 20 atoms per primitive cell). In order to minimize as much as
167 possible spurious interactions between the periodic images of the boron defects, the
168 unit-cell of the models was built from the 2x2x2 super-cells of calcite (rhombohedral
169 cell, 80 atoms) and aragonite (160 atoms) previously used in Balan et al. (2014). The
170 equilibrium geometry of these models was obtained by displacing the atoms up to a
171 minimum energy state, characterized by the fact that the forces experienced by the
172 atoms vanish. These structure relaxations were done using the PWscf code of the
173 Quantum ESPRESSO package (Giannozzi et al. 2009; http://www.quantum-
174 espresso.org) and forces on atoms were minimized to less than 10^{-4} Ry/a.u. The

175 Brillouin zone sampling was restricted to a single *k*-point; which is appropriate to treat
176 such systems with large unit-cell.
177 A reference theoretical sassolite (boric acid; $B(OH)_3$) structure was obtained
178 using a 2x2x2 *k*-points grid. The relaxed cell volume (V = 285.28 $Å^3$) and bond lengths
179 (d(B-O) = 1.378 Å; d(O-H) = 1.01 Å) slightly overestimate their experimental
180 counterparts (V = 273.62 $Å^3$; d(B-O) = 1.36 Å; d(O-H) = 0.9 Å; Zachariasen 1954), which
181 is consistent with a previous DFT-GGA modeling study (Ferlat et al. 2006). A theoretical
182 structure of takedaite ($Ca_3B_2O_6$) was also obtained with a 2x2x2 *k*-points grid, leading to
183 relaxed cell volume (V = 785.23 $Å^3$) and bond lengths (d(B-O) = 1.391 Å) slightly larger
184 than experimental values (V = 765.61 $Å^3$, d(B-O) = 1.384 Å; Vegas et al. 1975).
185
186 **2.2 First-principles metadynamics**
187
188 First-principles metadynamics (Laio and Parrinello 2002) runs were used to
189 determine the most stable configuration of $B(OH)_4^-$ in its crystal host from an
190 exploration of the free-energy landscape drawn by variations in the H-bonding pattern.
191 This approach provides an efficient method to explore a free-energy landscape
192 potentially displaying several relative minima separated by barriers higher than the
193 relevant thermal energy. Usual molecular dynamics would require prohibitively high
194 temperature and/or long simulation to achieve an adequate sampling of the
195 corresponding phase space. In contrast, the metadynamics builds an history dependent
196 bias potential which drives the system away from the previously explored
197 configurations, thus accelerating the exploration of the phase space and providing an
198 elegant way to pass the energy barriers. In practice, the bias potential is built in a space
199 of reduced dimensionality depending on the properties under study and referred to as

collective variables space. For example, a chemical reaction can be described by selecting a specific inter-atomic distance reflecting the breaking or the formation of a chemical bond. In the present study, exploring the different possible configurations of a given tetragonal boron group with respect to the calcite/aragonite crystal host equates to exploring different topologies in the network of chemical interactions formed by covalent and hydrogen bonds in a boron-centered region.

Born-Oppenheimer metadynamics runs were performed in the NVT ensemble (i.e. the number of atoms, volume and average temperature were constant during the runs) using the same DFT framework and parameters as those used for the structural relaxations. The hydrogen mass was increased to two atomic mass units and the runs were carried out with a timestep of 0.4×10^{-15} s. Temperature was controlled to 300 K employing a stochastic velocity rescaling thermostat (Bussi et al. 2007). Both in aragonite and calcite, we employed SPRINT collective variables (Pietrucci and Andreoni 2011), as implemented in Plumed (Bonomi et al., 2009), including a total of 26 atoms, namely the 4 hydrogens belonging to $B(OH)_4^-$ and 22 oxygens belonging to carbonates and lying within 4 Å of the oxygens belonging to $B(OH)_4^-$. The 26 collective variables were biased simultaneously adding every 100 molecular dynamics steps Gaussian hills of height 5.2 kJ/mol and width 0.9 or 1.1 (for aragonite or calcite, respectively).

To facilitate the identification of the different metastable configurations explored along the metadynamics trajectory, we performed a structural cluster analysis in the space of SPRINT collective variables, employing the k-medoids algorithm as implemented in the software piv-clustering (Gallet and Pietrucci 2013).

2.3 First-principles calculation of NMR parameters

The I = 3/2 nuclear spin of ^{11}B implies that its NMR properties involve both the Zeeman effect and the interaction of the nuclear quadrupolar moment with the electric field gradient at the nucleus. Accordingly, three parameters can be extracted from ^{11}B NMR spectra, namely the chemical shift δ_{iso}, the quadrupolar coupling constant C_Q and the asymmetry parameter η.

The NMR chemical shift describes the difference between the applied external magnetic field and the magnetic field at the nucleus positions. It can be obtained from the structural models by calculating the shielding of the nuclei relative to the electronic current induced by the external magnetic field. This current was calculated by using the GIPAW approach, which allows reconstructing the all-electron magnetic response from the pseudo-wave-functions (Pickard and Mauri 2001; Charpentier 2011; Bonhomme et al. 2012). The calculations were performed using the PWscf and GIPAW codes of the Quantum ESPRESSO package (Giannozzi et al. 2009). Norm-conserving pseudo-potentials were used and the wave functions kinetic energy cutoff was increased to 80 Ry. The integral over the Brillouin zone was done using a Monkhorst-Pack 1×1×1 *k*-point grid for the different models and 2×2×2 for sassolite ($B(OH)_3$) used as a reference. The isotropic chemical shift δ_{iso} is defined as $\delta_{iso} = -(\sigma - \sigma^{ref})$, where σ is the isotropic shielding (one-third of the trace of the NMR shielding tensor) and σ^{ref} is the isotropic shielding of the same nucleus in a reference system. In our calculations, absolute shielding tensors are obtained. To fix the scales, σ^{ref} was chosen by comparing experimental (19.2 ppm, Soraru et al. 1999) and calculated δ_{iso} values in $B(OH)_3$.

The C_Q and η parameters are related to the eigenvalues of the electric field gradient tensor and reflect the symmetry of the B environment. The C_Q = 2.49 MHz and η = 0.0 parameters computed for sassolite ($B(OH)_3$) are consistent with experimental

values (2.47 MHz and 0.0; Klochko et al. 2009). It should be noted that for the $C_Q(^{11}B)$ calculation, a quadrupole moment of 35 mb was used: this value is smaller than the theoretical value of 40 mb (Pyykkö, 2008) as recommended by Soleilhavoup et al. (2010) in borosilicate glasses. Estimated precision is ±0.5 ppm, ±0.1 MHz and ±0.1 for δ_{iso}, C_Q and η, respectively.

3. RESULTS

3.1 Trigonal boron incorporation at the carbonate site

We first consider the incorporation of trigonal boron species. The simplest model is obtained by substituting a B^{3+} for a C^{4+} (Table 1). The charge balance is obtained by spreading homogeneously an electrostatic counter-charge over the unit-cell. The crystal site symmetry is preserved. The three equivalent B-O bonds in calcite have a length of 1.388 Å. The BO_3^{3-} group in aragonite displays a mirror symmetry with a shorter B-O distance of 1.380 Å on the mirror plane and two symmetric B-O distances of 1.383 Å. The high symmetry of BO_3^{3-} groups in the homogeneously compensated models leads to very small η parameters. Compared to calcite, the aragonite ^{11}B chemical shift is higher and similar to that of the calcium orthoborate, takedaite.

A more realistic charge compensation mechanism consists in adding one H atom to the previous system, forming a $BO_2(OH)^{2-}$ group (Fig. 1). For the 3-fold calcite site, the three oxygen atoms are symmetrically equivalent and only one protonation scheme was considered. Two different protonation schemes are considered for aragonite, affecting the oxygen on the mirror plane of the BO_3 triangle (scheme A) or one of the other two symmetric oxygen atoms (scheme B). Scheme A is more stable than B by 16.8 kJ/mol

and should be thermodynamically dominant at room temperature. The $BO_2(OH)^{2-}$ species in calcite and aragonite display similar structural characteristics. The OH group points out of the BO_3 triangle sharing a H-bond of moderate strength with an oxygen belonging to an adjacent carbonate group. A significant distortion of the trigonal geometry is observed with the B-O(H) distance increasing by ~ 0.1 Å; whereas the two other B-O distances decrease by 0.03 to 0.04 Å. Compared to the models with an homogeneous charge compensation, the ^{11}B δ_{iso} decreases by 1.5 and by 3 to 4 ppm in calcite and aragonite, respectively; whereas the quadrupolar coupling parameter C_Q is weakly affected. The asymmetry parameter η increases to 0.8 indicating a strong departure from the revolution symmetry, consistent with the in-plane distortion of the BO_3 triangle.

3.2 Tetragonal boron incorporation at the carbonate site

Following an approach similar to that applied to the trigonal B species, $B(OH)_4^-$ for CO_3^{2-} substitution was modeled by using a homogeneous electrostatic background to compensate the charge imbalance. Previous calculations on sulfate incorporation in carbonate (Balan et al. 2014) provided a suitable starting guess for the structural optimization. However, the large number of potential H-bond acceptors around the impurity increases the probability to drive the system to a metastable configuration. This difficulty was circumvented by performing first-principles metadynamics (FPM) runs (Laio and Parrinello 2002; Pietrucci and Andreoni 2011) to explore the free energy landscape of the borate group conformation and to isolate the most favorable one.

The aragonite FPM run lasted ~ 6 x 10^{-12} s (Fig. 2, video file in electronic annex). In an initial phase of ~3 x 10^{-12} s the instantaneous bias potential fluctuates between

299 zero and less than 10 kJ/mol, indicating that different configurations are being explored
300 (zero bias corresponds to an unexplored region of the configuration space). In a second
301 phase, the bias potential starts to grow more consistently to few tens of kJ/mol without
302 coming back to zero. This indicates that the available low-energy configurations have
303 been exhausted and that higher-energy configurations have been explored.
304 Concomitantly, the fluctuations of the SPRINT topological variables related to H and O
305 atoms (Fig. 2) attest to the changes of configuration of the $B(OH)_4^-$ species, by
306 reorienting the OH groups to engage in different patterns of hydrogen bonds with the
307 carbonates. The trajectory analysis leads to 8 maximally distinct instantaneous
308 configurations. After structural optimization, two classes of configurations differing by
309 the orientation of the O3-H bond (almost parallel to the b- axis or to the c-axis), could be
310 defined. In the following, only the most stable configuration will be considered since the
311 energy difference between the two (19 kJ/mol) is significantly larger than the typical
312 thermal energy at ambient temperature (2.5 kJ/mol). In this configuration (Fig. 1), the
313 O3-H bond is almost parallel to the c-axis and the borate group is slightly distorted with
314 an average B-O length of 1.481 Å (Table 1). As for sulfate (Balan et al. 2014), the borate
315 group is tilted with respect to the (a,b) plane and a significant displacement of the
316 neighboring carbonate groups is observed. The four H-bonds display quite regular
317 characteristics with O-H distances ranging from 0.989 to 1.008 Å and O(H)...O distances
318 from 2.62 to 2.65 Å. Few relative energy minima were however observed in each
319 configuration class due to moderate displacements of the surrounding carbonates,
320 leading to energy differences ranging between 5 and 13 kJ/mol. These configurations
321 can be envisioned as intermediate states in the transition from one H-bonding geometry
322 to the other. A longer FPM run (15×10^{-12} s, Fig. 3, video file in electronic annex) was
323 performed on calcite but only two different instantaneous configurations were

identified, leading to a single relaxed structure. As observed for other tetrahedral anions in calcite (Reeder et al. 1994; Fernandez-Diaz et al. 2010; Balan et al. 2014), the $B(OH)_4^-$ anion is slightly tilted with the apical B-O bond forming an angle of 13° with respect to the ternary axis of calcite. Although the structural environment is different, only slight differences in the B-O and H-bond distances are observed between calcite and aragonite (Table 1). The theoretical ^{11}B NMR parameters of $B(OH)_4^-$ in calcite and aragonite are similar, with δ_{iso} close to 1 ppm and small quadrupolar coupling parameters (Table 1).

As for the trigonal B species, alternative models of tetragonal borate in calcium carbonates were explored by assuming local charge compensation mechanisms. Removing a proton from the $B(OH)_4^-$ group, modifies its charge to -2 (equivalent to that of the CO_3^{2-} group). Starting from the tetrahedral geometries obtained from FPM runs, four relaxed schemes (matching the four different H atoms of the borate group) are obtained for each calcium carbonate polymorph. The deprotonation of the O3-H group (Table 1) is favored in aragonite by more than 27 kJ/mol. In calcite, the most stable (by more than 7 kJ/mol) configuration is obtained by deprotonation of the O2-H group (Table 1). All the $BO(OH)_3^{2-}$ species display a significant distortion of the boron coordination shell. Consistently, the C_Q values increase, ranging between 1.01 and 1.53 MHz.

A different mechanism ensuring the neutrality of $B(OH)_4^-$ for CO_3^{2-} substitution corresponds to the coupled substitution of a monovalent cation for Ca^{2+}. Sodium is the most relevant one both in terms of seawater abundance and ionic radii similarity. Two configurations have been selected by assuming that the Na^+ for Ca^{2+} substitution affects the site closest to the central boron atom (Fig. 1). In both configurations, the structure of the $B(OH)_4^-$ group and the H-bonding pattern is weakly affected by the Na^+ for Ca^{2+} substitution. The Na to B distances increase by ~0.05 Å compared to Ca to B distances.

Compared with the homogeneously compensated models, only weak variations of the ^{11}B NMR parameters are observed (Table 1).

4. DISCUSSION

4.1 Boron in calcium carbonates: Comparing theory and experiment

4.1.1 Trigonal boron speciation

Although only few studies report experimentally determined NMR parameters of boron in calcite and aragonite, they reveal a significant variability of the trigonal boron environment (Table 2, Fig. 4). The chemical shift of trigonal boron ranges from 16 ppm (calcite) to 22 ppm (heated aragonite) and strong differences are observed on the rhombic η parameter. The trigonal boron species in the calcite samples investigated by Sen et al. (1994) is rhombically distorted, with η values of 0.67 and 0.5 in the synthetic and biogenic sample, respectively. In contrast, the nil η values reported by Klochko et al. (2009) in biogenic calcite and aragonite samples correspond to a radially symmetric environment of boron. A similarly low value of η is reported by Rollion-Bard et al. (2011) for a biogenic aragonitic coral sample. As already highlighted by Klochko et al. (2009), these variations in η values are highly significant because η is only defined between 0 and 1.

The theoretical parameters determined for the $BO_2(OH)^{2-}$ species in calcite are consistent with those reported by Sen et al. (1994) for synthetic calcite. The chemical shift and quadrupolar coupling of $BO_2(OH)^{2-}$ in aragonite also match the experimental values reported by Mavromatis et al. (2015) for synthetic aragonite. Unfortunately, the η

parameter was not reported for this sample, likely because of its low trigonal B content. From the comparison of theoretical and experimental NMR parameters, singly protonated $BO_2(OH)^{2-}$ groups appear as the dominant speciation of trigonal boron in the synthetic calcium carbonates precipitated from solutions. This confirms the previous suggestions that trigonal boron in carbonates should be distorted and partially deprotonated (Hemming and Hanson 1992; Tossell 2005). This speciation is favored by the electrostatic balance requirements. An overall preference for local electrostatic charge compensation in minerals is attested by the observation of chemically complex defects, associating different trace elements in the same crystal site. For example, clumped-defects associating fluoride ions with carbonate groups have been observed in apatite (Yi et al. 2013). Note however that, in absence of C_Q and η values, some uncertainty affects the interpretation of the NMR parameters reported by Mavromatis et al. (2015) for synthetic calcite samples. Their chemical shift is only slightly lower than that of $BO_2(OH)^{2-}$ species and consistent with the value reported by Sen et al. (1994) for a synthetic calcite sample (Fig. 4). Isotopic compositions (Noireaux et al. 2015) indicate (under the assumption that no isotope fractionation occurs during incorporation) that between 20% and 40% of boron in these samples results from the incorporation of aqueous boric acid and that this proportion is linearly correlated with the pH-dependent amount of boric acid in solution. The proportion of trigonal B detected by NMR is however higher than that inferred from isotopic composition (Noireaux et al., 2015). Thus, both borate anions and boric acid molecules could contribute to the incorporation of $BO_2(OH)^{2-}$ species in the bulk of calcite particles. This implies a coordination change of tetragonal borate as well as several deprotonation steps affecting the tetragonal and trigonal boron species in the interfacial region of growing calcite crystals.

Concerning the biogenic calcium carbonates, the algal calcite investigated by Sen et al. (1994) displays NMR parameters consistent with $BO_2(OH)^{2-}$ groups. In contrast, the parameters reported by Klochko et al. (2009) for a foram calcite correspond to fully deprotonated BO_3^{3-} groups substituted in the calcite structure (Fig. 4, Table 1). The sensitivity of ^{11}B NMR to the trigonal boron protonation state is further confirmed by the higher δ_{iso}, and weak η, indicative of a more symmetric boron environment in a calcite sample produced by the high-temperature (500 °C) transformation of biogenic aragonite. These parameters are close to those computed for BO_3^{3-} groups in aragonite (Fig. 4) and in the calcium orthoborate takedaite (Table 1). They indicate that the thermally driven aragonite to calcite transformation leads to a full deprotonation of borate groups. They however suggest that the local environment of BO_3^{3-} groups in the heated aragonite differs from that in crystalline calcite.

The ^{11}B NMR parameters of trigonal boron in coral aragonitic samples combine comparatively low δ_{iso} value and weak η (Klochko et al. 2009; Rollion-Bard et al. 2011). The weak η is indicative of a regular coordination shell, but the δ_{iso} values are too low to correspond to fully deprotonated BO_3^{3-} groups (Fig. 4; Table 1). Accordingly, these parameters are interpreted as related to fully protonated $B(OH)_3$ molecules. The incorporation of boric acid molecules in crystallographic sites is unrealistic because of the corresponding strong electrostatic charge imbalance. It is more likely that $B(OH)_3$ molecules are directly scavenged from the solution and encapsulated by the solid phase. Such step can involve their incorporation in the amorphous and hydrous calcium carbonate phases, observed under high supersaturation and elevated growth rate conditions and identified as intermediate phases in the growth of biogenic calcium carbonates (e.g. Gower 2008; Purgstaller et al., 2016). The $B(OH)_3$ molecules could also occur in interfacial or porous regions separating ordered $CaCO_3$ nanodomains, such as

423 those observed in calcitic red coral (Vielzeuf et al. 2008). The preserved coordination
424 state and isotopic composition can lead to higher than expected $\delta^{11}B$, depending on the
425 proportion of $B(OH)_3$ molecules relative to the total B content. This interpretation is
426 consistent with the concomitant observation of elevated $\delta^{11}B$ and higher trigonal boron
427 concentration at the center of calcification of an aragonitic coral sample by Rollion-Bard
428 et al. (2011). Note however that trigonal B usually is a minority species in aragonitic
429 samples, which tempers the isotopic effect related to $B(OH)_3$ incorporation.
430
431 4.1.2 Tetragonal boron speciation
432
433 The experimental chemical shift of tetragonal B species displays a range of
434 variation between -2.4 and 3 ppm, considering both calcite and aragonite (Fig. 5). Except
435 two samples with δ_{iso} above 2 ppm and two signals with negative chemical shifts
436 ascribed to non-structural species in calcitic samples (Mavromatis et al. 2015), the NMR
437 parameters are consistent with those obtained for the $B(OH)_4^-$ models. The
438 systematically nil values of experimental quadrupolar coupling parameters (Table 2)
439 attest to a highly symmetric B environment. They rule out the partially deprotonated
440 tetragonal species, which are characterized by theoretical C_Q values larger than 1 MHz.
441 Accordingly, tetragonal B should mostly occur in the calcium carbonate samples as fully
442 protonated $B(OH)_4^-$ groups. A high protonation state of tetragonal B was suggested by
443 Klochko et al. (2009) from ^1H decoupling experiments.
444 The substitution of $B(OH)_4^-$ for CO_3^{2-} implies that more remote mechanisms
445 ensure the charge compensation, among which the Na^+ for Ca^{2+} substitution is the most
446 probable one. As a matter of fact, the Na-bearing models also display NMR parameters
447 consistent with the experimental observations. This coupled substitution could be

448 responsible, at least in part, for the dependence of B/Ca ratio on salinity reported for
449 biogenic calcium carbonates (Allen et al. 2011, 2012; Allen and Hönisch 2012; Henehan
450 et al. 2015). Inorganic co-precipitation experiments of Kitano et al. (1978) have also
451 shown a significant increase in B incorporation in calcite with increasing NaCl
452 concentration in the parent solution. For aragonite, the observed dependence was in the
453 opposite direction but with a comparatively weaker magnitude. We note however that
454 an aragonitic coral sample and an hydrothermal calcitic sample investigated by Klochko
455 et al. (2009) display higher δ_{iso} values of 2.54 and 2.87 ppm, respectively, and likely
456 correspond to $B(OH)_4^-$ groups in a different environment or involving a charge
457 compensation mechanism differing from that prevailing in the other samples. The
458 potential presence of contaminant phases cannot be fully excluded for these natural
459 samples. Beside Na^+ for Ca^{2+} substitution, different charge compensation mechanisms
460 could occur, as shown by the Na-free synthesis experiments of Hemming et al. (1995)
461 and Sen et al. (1994). For example, HCO_3^- groups associated with Ca vacancies could play
462 such compensation role. A potential role of phosphate anions substituted for carbonate
463 groups has also been suggested by Henehan et al. (2015). Variations in the borate group
464 environment are also attested by the broad signals with slightly negative chemical shifts
465 observed by Mavromatis et al. (2015), interpreted as corresponding to a fraction of
466 borate groups occurring in defective domains of the calcite samples.
467
468 **4.2 Boron speciation in calcium carbonates: Implications for the paleo-pH proxy**
469
470 The present results show that B in calcium carbonates does occur as substituted
471 species for CO_3^{2-} anions, thus confirming its structural nature. They further show that its
472 speciation depends on the polymorph considered. This is fully consistent with a number

of previous studies on boron incorporation in biogenic and abiotic carbonates (e.g. Klochko et al. 2009; Mavromatis et al. 2015; Noireaux et al. 2015) and strongly challenge the hypothesis on which the use of boron isotopes to reconstruct paleo ocean pH has been used (i.e. sole incorporation of the aqueous borate ion). In calcite, structural boron is present as partially deprotonated trigonal $BO_2(OH)^{2-}$ species, coexisting with substituted $B(OH)_4^-$ groups in a proportion depending on the crystal growth parameters. In aragonite, the $B(OH)_4^-$ substitution for CO_3^{2-} anions is dominant. The theoretical modeling of NMR spectra also indicates that different B species, including entrapped $B(OH)_3$ molecules and substituted BO_3^{3-} groups can occur in biogenic samples. The diversity of B speciation indirectly confirms the importance of out-of-equilibrium parameters and interfacial properties in determining the chemical form and abundance of boron in calcium carbonate (e.g., Hemming et al. 1998; Hobbs and Reardon 1999; Ruiz-Agudo et al. 2012; Gabitov et al. 2014; Branson et al. 2015; Noireaux et al. 2015; Uchikawa et al. 2015; Kaczmarek et al. 2016). Although the $B(OH)_3$ molecules in biogenic aragonitic samples might have been directly scavenged from the solution, the other trigonal $BO_2(OH)^{2-}$ and BO_3^{3-} species most probably result from a coordination change and deprotonation of boron species adsorbed at the mineral surface.

An important implication of the observed diversity of B speciation in calcium carbonates is that the ratio of trigonal to tetragonal species determined by NMR spectroscopy is not a sufficient parameter to infer its incorporation mechanism. This ratio is not simply related to the trigonal to tetragonal proportion in the solution nor solely results from a coordination decrease affecting the adsorbed borate ion during its incorporation in the crystal structure. The environment and protonation state of trigonal B however appears as more variable than that of the tetragonal species. In this latter case, the variations are most likely related to more remote charge compensation

498 mechanisms and do not affect the first coordination shell of boron. In addition, the high
499 sodium concentration of seawater could favor the Na^+ for Ca^{2+} substitution in the charge
500 compensation of $B(OH)_4^-$ species. The prevalence of a specific charge compensation
501 mechanism would reduce the crystal-chemical complexity of the $B(OH)_4^-$ incorporation
502 mechanism. Interestingly, the affinity of aragonite is higher than that of calcite for both B
503 and Na. In the case of Na, this has been interpreted as reflecting its incorporation in
504 interstitial sites of calcite, instead of structural Ca site as in aragonite (Ishikawa and
505 Ichikuni 1984; Okumura et al. 1986). As a consequence, aragonitic samples in which
506 tetragonal B is dominant should faithfully reflect the pH of past oceans, as proposed by
507 Noireaux et al. (2015), provided that sampling strategies taking into account the growth
508 mechanism of biologic aragonite are developed (Rollion-Bard et al. 2011).

509 In the case of calcitic samples, the more diverse boron speciation could be
510 considered as a fingerprint of the growth mechanism and could serve as an indicator to
511 extrapolate the laboratory calibrations to the geologic samples. The recent spatially-
512 resolved study of Branson et al. (2015) indicates a dominantly trigonal (>85%)
513 coordination and a heterogeneous distribution of boron in foraminiferal calcite;
514 whereas NMR studies revealed a fraction of tetragonal B in biogenic calcite (~20%, Sen
515 et al. 1994; ~54%, Klochko et al. 2009). Thus, the occurrence of differently coordinated
516 species, with potentially distinct isotopic compositions, in spatially different domains of
517 the composite biogenic samples cannot be excluded. As diagenesis and alteration may
518 differently affect these domains, the boron isotopic composition of geological samples
519 would then depend on their preservation state (Wara et al. 2003). We note however that
520 the observations of Edgar et al. (2015) suggest that the boron isotopic composition of
521 fossil planktonic foraminiferal calcite is resistant to diagenetic transformations. This

calls for further experimental studies focusing on the effects of diagenesis on boron speciation in carbonates.

Finally, we highlight that the approach developed in the present study, which combines a metadynamics determination of stable configurations of polyatomic groups with the first-principles calculation of related spectroscopic parameters, represents a general tool to explore the speciation of molecular anions in host crystalline matrices, readily applicable to a larger range of geochemical proxies in minerals.

ACKNOWLEDGMENTS

This work has been supported by the French National Research Agency through the CARBORIC (ANR-13-BS06-0013-06) project. This work was performed using HPC resources from GENCI-IDRIS (Grants i2016041519 and i2016097535). We thank M. Henehan and two anonymous reviewers for their constructive comments and suggestions.

REFERENCES

Allen K. A. and Hoenisch B. (2012) The planktic foraminiferal B/Ca proxy for seawater carbonate chemistry: A critical evaluation, *Earth Planet. Sci. Lett.* **345–348**, 203–21.

Allen K. A., Hoenisch B., Eggins S. M., Yu J., Spero H. J. and Elderfield H. (2011) Controls on boron incorporation in cultured tests of the planktic foraminifer Orbulina universa, *Earth Planet. Sci. Lett.* **309**, 291–30.

545 Allen K. A., Hoenisch B., Eggins S. M. and Rosenthal Y. (2012) Environmental controls on
546 B/Ca in calcite tests of the tropical planktic foraminifer species Globigerinoides
547 ruber and Globigerinoides sacculifer, *Earth Planet. Sci. Lett.* **351–352**, 270–280,
548 Balan E., Blanchard M., Pinilla C. and Lazzeri M. (2014) First-principles modeling of
549 sulfate incorporation and $^{34}S/^{32}S$ isotopic fractionation in different calcium
550 carbonates. *Chem. Geol.* **374-375**, 84-91.
551 Bonhomme C., Gervais C., Babonneau F., Coelho C., Pourpoint F., Azaïs T., Ashbrook S.E.,
552 Griffin J.M., Yates J.R., Mauri F. and Pickard C.I. (2012) First-Principles Calculation
553 of NMR Parameters using the gauge including projector augmented wave method:
554 A chemist's point of view. *Chemical reviews* **112**, 5733–5779.
555 Bonomi M., Branduardi D., Bussi G., Camilloni C., Provasi D., Raiteri P., Donadio D.,
556 Marinelli F., Pietrucci F., Broglia R.A. and Parrinello M. (2009) PLUMED: a portable
557 plugin for free-energy calculations with molecular dynamics. *Comp. Phys. Comm.*
558 **180**, 1961.
559 Branson O., Kaczmarek K., Refern S. A. T., Misra, S., Langer G., Tyliszczak T., Bijma J. and
560 Elderfield H. (2015) The coordination and distribution of B in foraminiferal calcite.
561 *Earth Planet. Sci. Lett.* **416**, 67-72.
562 Bussi G., Donadio D. and Parrinello M. (2007) Canonical sampling through velocity
563 rescaling. *J. Chem. Phys.* **126**, 014101.
564 Charpentier T. (2011) The PAW/GIPAW approach for computing NMR parameters: A
565 new dimension added to NMR study of solids. *Solid State NMR* **40**, 1-20.
566 Cygan, R.T. and Kubicki, J.D. (2001) Reviews in Mineralogy and Geochemistry: Molecular
567 Modeling Theory: Applications in the Geosciences. 531 p. The Mineralogical
568 Society of America, Washington, D.C.

569 Edgar K., Anagnostou E., Pearson P. and Foster G. (2015) Assessing the impact of
570 diagenesis on 11B, 13C, 18O, Sr/Ca and B/Ca values in fossil planktic foraminiferal
571 calcite. *Geochim. Cosmochim. Acta* **166**, 189- 209.
572 Ferlat G., Cormier L., Mauri F., Balan E., Charpentier T., Anglada E. and Calas G. (2006)
573 Ab initio calculations on borate systems. *Eur. J. Glass Sci. Techno. B* **4**, 441-444.
574 Fernández-Díaz L., Fernández-González A. and Prieto M. (2010) The role of sulfate
575 groups in controlling $CaCO_3$ polymorphism. *Geochim. Cosmochim. Acta* **74**, 6064-
576 6076.
577 Gabitov R. I., Rollion-Bard C., Tripati A. and Sadekov A. (2014) In situ study of boron
578 partitioning between calcite and fluid at different crystal growth rates. *Geochim.*
579 *Cosmochim. Acta* **137**, 81-92.
580 Gaillardet J. and Allègre C.J. (1995) Boron isotopic compositions of corals: Seawater or
581 diagenesis record? *Earth Planet. Sci. Lett.* **136**, 665-676.
582 Gallet G. A. and Pietrucci F. (2013) Structural cluster analysis of chemical reactions in
583 solution. *J. Chem. Phys.* **139**, 074101.
584 Garrity K. F., Bennett J. W., Rabe K. M. and Vanderbilt D. (2014) Pseudopotentials for
585 high-throuhput DFT calculations. *Comput. Mat. Sci.* **81**, 446-452.
586 Giannozzi P., Baroni S., Bonini N., Calandra M., Car R., Cavazzoni C., Ceresoli D., Chiarotti
587 G.L., Cococcioni M., Dabo I., Dal Corso A., de Gironcoli S., Fabris S., Fratesi G.,
588 Gebauer R., Gerstmann U., Gougoussis C., Kokalj A., Lazzeri M., Martin-Samos L.,
589 Marzari N., Mauri F., Mazzarello R., Paolini S., Pasquarello A., Paulatto L., Sbraccia
590 C., Scandolo S., Sclauzero G., Seitsonen A.P., Smogunov A., Umari P. and
591 Wentzcovitch R.M. (2009) Quantum ESPRESSO: a modular and open-source
592 software project for quantum simulations of materials. *J. Phys.: Cond. Matt.* **21**,
593 395502.

Gower L. B. (2008) Biomimetic model systems for investigating the amorphous precursor pathway and its role in biomineralization. *Chem. Rev.* **108**, 4551–4627.

Henehan M. J., Foster G. L., Rae J. W. B., Prentice K. C., Erez J., Bostock H. C., Marshall B. J. and Wilson P. A. (2015) Evaluating the utility of B/Ca ratios in planktic foraminifera as a proxy for the carbonate system: A case study of Globigerinoides ruber. *Geochem. Geophys. Geosyst*. **16**, 1052–1069

Hemming N. G. and Hanson G. N. (1992) Boron isotopic composition and concentration in modern marine carbonates. *Geochim. Cosmochim. Acta* **56**, 537-543.

Hemming N. G., Reeder R. J. and Hanson G. N. (1995) Mineral-fluid partitioning and isotopic fractionation of boron in synthetic calcium carbonates. *Geochim. Cosmochim. Acta* **59**, 371-379.

Hemming N. G., Reeder R. J. and Hart S. R. (1998) Growth-step-selective incorporation of boron on the calcite surface. *Geochim. Cosmochim. Acta* **62**, 2915-2922.

Hobbs M. Y. and Reardon E. J. (1999) Effect of pH on boron coprecipitation by calcite: Further evidence for nonequilibrium partitioning of trace elements. *Geochim. Cosmochim. Acta* **63**, 1013-1021.

Ishikawa M. and Ichikuni M. (1984) Uptake of sodium and potassium by calcite. *Chem. Geol.* **42**, 137-146

Kaczmarek K., Nehrke G., Misra S., Bijma J. and Elderfield H. (2016) Investigating the effects of growth rate and temperature on the B/Ca ratio and $\delta^{11}B$ during inorganic calcite formation. *Chem. Geol.* **421**, 81-92.

Kitano Y., Okumura M. and Idogaki (1978) Coprecipitation of borate-born with calcium carbonate. *Geochemical Journal* **12**, 183-189.

Klochko K., Kaufman A. J., Yao W., Byrne R. H. and Tossell J. A. (2006) Experimental measurement of boron isotope fractionation in seawater. *Earth Planet. Sci. Lett.*

248, 276-285.

Laio A. and Parrinello M. (2002) Escaping free-energy minima. *Proc. Nat. Acad. Sci.* **99**, 12562-12566.

Liu Y. and Tossell J. A. (2005) Ab initio molecular orbital calculations for boron isotope fractionations on boric acids and borates. *Geochim. Cosmochim. Acta* **69**, 3995-4006.

Lemarchand D., Gaillardet J., Lewin E. and Allègre C. J. (2002) Boron isotope systematics in large rivers: implications for the marine boron budget and paleo-pH reconstruction over the Cenozoic. *Nature* **408**, 951-954.

Martinez-Boti M. A., Marino G., Foster G. L., Ziveri P., Henehan M.J., Rae J. W. B., Mortyn P. G. and Vance D. (2015) Boron isotope evidence for oceanic carbon dioxide leakage during the last deglaciation. *Nature* **518**, 219-222.

Mavromatis V., Montouillout V., Noireaux J., Gaillardet J. and Schott J. (2015) Characterization of boron incorporation and speciation in calcite and aragonite from co-precipitation experiments under controlled pH, temperature and precipitation rate *Geochim. Cosmochim. Acta* **150**, 299-313.

Nir O., Vengosh A., Harkness J. S., Dwyer G. S. and Lahav O. (2015) Direct measurement of the boron isotope fractionation factor: Reducing the uncertainty in reconstructing ocean paleo-pH. *Earth Planet. Sci. Lett.* **414**, 1-5.

Noireaux J., Mavromatis V., Gaillardet J., Schott J., Montouillout V., Louvat P., Rollion-Bard C. and Neuville D. R. (2015) Crystallographic control on the boron isotope paleo-pH proxy. *Earth Planet. Sci. Lett.* **430**, 398-407.

Okumura M. and Kitano Y. (1986) Coprecipitation of alkali metal ions with calcium carbonate. *Geochim. Cosmochim. Acta* **50**, 49-58.

643 Pagani M., Lemarchand D., Spivack A and Gaillardet J. (2005) A critical evaluation of the
644 boron isotope-pH proxy: the accuracy of ancient ocean pH estimates. *Geochim.*
645 *Cosmochim. Acta* **69**, 953–961.
646 Palmer M. R., Pearson P. N. and Cobb S. J. (1998) Reconstructing past ocean pH-depth
647 profiles. *Science* **282**, 1468-1471.
648 Pearson P. N. and Palmer M. R. (1999) Middle eocene seawater pH and atmospheric
649 carbon dioxide concentrations. *Science* **284**, 1824-1826.
650 Pearson P. N., Foster G. L. and Wade B. S. (2009) Atmospheric carbon dioxide through
651 the Eocene-Oligocene climate transition. *Nature* **461**, 1110–1113.
652 Perdew J. P., Burke K. and Ernzerhof M. (1996) Generalized gradient approximation
653 made simple. *Phys. Rev. Lett.* **77**, 3865–3868.
654 Pickard C. and Mauri F. (2001) All-electron magnetic response with pseudopotentials:
655 NMR chemical shifts. *Phys. Rev. B* **63**, 245101.
656 Pietrucci F. and Andreoni W. (2011) Graph theory meets ab initio molecular dynamics:
657 atomic structures and transformations at the nanoscale. *Phys. Rev. Lett.* **107**,
658 085504.
659 Purgstaller B., Mavromatis V., Immenhauser A. and Dietzel M. (2016) Transformation of
660 Mg bearing amorphous calcium carbonate to Mg-calcite - In situ monitoring.
661 *Geochim. Cosmochim. Acta* **174**, 180-195.
662 Pyykkö P. (2008) Year-2008 nuclear quadrupole moments. *Mol. Phys.* **106**, 1065.
663 Reeder R. J., Lamble G. M., Lee J.-F. and Staudt W. J. (1994) Mechanism of SeO_4^{2-}
664 substitution in calcite: An XAFS study. *Geochim. Cosmochim. Acta* **58**, 5639-5646.
665 Rollion-Bard C., Blamart D., Trebosc J., Tricot G., Mussi A. and Cuif J.-P. (2011) Boron
666 isotops as a pH proxy: A new look at boron speciation in deep-sea corals using ^{11}B
667 MAS NMR and EELS. *Geochim. Cosmochim. Acta* **75**, 1003-1012.

668 Ruiz-Agudo E., Putnis C. V., Kowacz M., Ortega-Huertas M. and Putnis A. (2012) Boron
669 incorporation into calcite during growth: Implications for the use of boron in
670 carbonates as a pH proxy. *Earth Planet. Sci. Lett.* **345-348**, 9-17.
671 Rustad J. R., Bylaska E. J., Jackson V. E. and Dixon D. A. (2010) Calculation of boron-
672 isotope fractionation between $B(OH)_{3(aq)}$ and $B(OH)_{4^-(aq)}$. *Geochim. Cosmochim. Acta*
673 **74**, 2843-2850.
674 Sanyal A., Hemming N. G., Hanson G. N. and Broecker W. S. (1995) Evidence for a higher
675 *p*H in the glacial ocean from boron isotopes in foraminifera. *Nature* **373**, 234–236.
676 Sen S., Stebbins J. F., Hemming N. G. and Ghosh B. (1994) Coordination environments of
677 B impurities in calcite and aragonite polymorphs: A ^{11}B MAS NMR study. *Am.*
678 *Mineral.* **79**, 819-825.
679 Soleilhavoup A., Delaye J.-M., Angeli F., Caurant D. and Charpentier T. (2010)
680 Contribution of first-principles calculations to multinuclear NMR analysis of
681 borosilicate glasses. *Magn. Reson. Chem.* **48**, S159–S170.
682 Soraru G.D., Babonneau F., Gervais C. and Dallabona N. (2000) Hybrid $RSiO1{:}5/B_2O_3$ gels
683 from modified silicon alkoxides and boric acid. *J. Sol-Gel Sci. and Techno.* **18**, 11–19.
684 Spivack A. J., You C. and Smith H. J. (1993) Foraminiferal boron isotope ratios as a proxy
685 for surface ocean pH over the past 21 Myr. *Nature* **363**, 149-151.
686 Tossell J. A. (2005) Boric acid, "carbonic" acid, and N-containing oxyacids in aqueous
687 solution: Ab initio studies of structure, pKa, NMR shifts, and isotopic fractionations.
688 *Geochim. Cosmochim. Acta* **69**, 5647-5658.
689 Tossell J. A. (2006) Boric acid adsorption on humic acids: Ab initio calculation of
690 structures, stabilities, ^{11}B NMR and ^{11}B,^{10}B isotopic fractionations of surface
691 complexes. *Geochim. Cosmochim. Acta* **70**, 5089-5103.

692 Uchikawa J., Penman D. E., Zachos J. C. and Zeebe R. E. (2015) Experimental evidence of
693 kinetic effects on B/Ca in synthetic calcite: Implications for potential $B(OH)_4^-$ and
694 $B(OH)_3$ incorporation. *Geochim. Cosmochim. Acta* **150**, 171-191.
695 Vegas A., Cano F. H. and Garcia-Blanco S. (1975) The crystal structure of calcium
696 orthoborate: a redetermination. *Acta Crystallogr B* **31**, 1416-1419.
697 Vengosh A., Kolodny Y., Starinsky A., Chivas A. R. and McCulloch M. T. (1991) Copre-
698 cipitation and isotopic fractionation of boron in modern biogenic carbonates.
699 *Geochim. Cosmochim. Acta* **55**, 2901–2910.
700 Vielzeuf D., Garrabou J., Baronnet A., Grauby O. and Marschal C. (2008) Nano to
701 macroscale biomineral architecture of red coral (Corallium rubrum). *Amer.*
702 *Mineral.* **93**, 1799–1815.
703 Wara M. W., Delaney M. L., Bullen T. D. and Ravelo A. C. (2003) Possible roles of pH,
704 temperature, and partial dissolution in determining boron concentration and
705 isotopic composition in planktonic foraminifera. *Paleoceanography* **18(4)**, 1100,
706 doi:10.1029/2002PA000797
707 Xiao Y. K., Li H. L., Liu W. G., Wang X. F. and Jiang S. Y. (2008) Boron isotopic fractionation
708 in laboratory inorganic carbonate precipitation: Evidence for the incorporation of
709 $B(OH)_3$ into carbonate. *Sci. China Ser. D* **51**, 1776–1785.
710 Yi H., Balan E., Gervais C., Segalen L., Fayon F., Roche D., Person A., Morin G., Guillaumet
711 M., Blanchard M., Lazzeri M. and Babonneau F. (2013) A carbonate-fluoride defect
712 model for carbonate-rich fluorapatite. *Amer. Mineral.* **98**, 1066-1069.
713 Zachariasen W. H. (1954) The precise structure of orthoboric acid. *Acta Crystallogr.* **7**,
714 305-310.
715 Zeebe R. E. (2005) Stable boron isotope fractionation between dissolved $B(OH)_3$ and $B(OH)_4^-$
716 *Geochim. Cosmochim. Acta* **69**, 2753–2766.

717

718 Table 1: Structural and ^{11}B NMR parameters of boron-bearing calcium carbonate models

B coordinence	mineral	model	B-O bond length (Å)	O-H bond length (Å)	δ_{iso} (ppm)	C_Q (MHz)	η
trigonal	calcite	BO_3^{3-}	1.388 (x3)	-	19.10	2.73	0.00
		$BO_2(OH)^{2-}$	1.345 1.350 O(H) 1.491	- - 0.995	17.51	2.59	0.84
	aragonite	BO_3^{3-}	1.380 1.383 (x2)	-	22.04	2.74	0.04
		$BO_2(OH)^{2-}$ (A)	1.343 1.350 O(H) 1.472	- - 0.988	19.11	2.59	0.81
		$BO_2(OH)^{2-}$ (B)	1.347 1.349 O(H) 1.472	- - 0.991	18.14	2.57	0.82
	takedaite	BO_3^{3-}	1.391	-	22.11	2.74	0.00
tetragonal	calcite	$B(OH)_4^-$	O1 1.438 O3 1.477 O4 1.489 O2 1.510	1.005 1.002 0.997 0.996	1.05	0.43	0.57
		$BO(OH)_3^{2-}$	O2 1.402 O1 1.494 O3 1.524 O4 1.532	- 0.996 0.996 0.994	1.29	1.09	0.34
		$B(OH)_4^-,Na^+$	O1 1.434 O3 1.470 O4 1.499 O2 1.522	1.006 0.993 0.997 0.992	1.15	0.56	0.67
	aragonite	$B(OH)_4^-$	O2 1.455 O1 1.476 O4 1.497 O3 1.497	0.992 1.008 0.989 1.003	0.81	0.22	0.50
		$BO(OH)_3^{2-}$	O3 1.402 O2 1.492 O1 1.530 O4 1.543	- 0.987 1.001 0.985	1.02	1.15	0.26
		$B(OH)_4^-,Na^+$	O2 1.457 O1 1.455 O3 1.501 O4 1.514	0.990 1.005 0.992 0.989	0.88	0.38	0.58

719

720

721

722

723 Table 2: Experimental ^{11}B NMR parameters of synthetic and natural calcium carbonates

B coordinence		sample	δ_{iso} (ppm)	C_Q (MHz)	η	ref.*	present interpretation
trigonal	synthetic	calcite	17.1 ±1	3.0 ±0.3	0.67 ±0.05	1	$BO_2(OH)^{2-}$
		heated aragonite	22.0 ±1	2.7 ±0.3	0.2 ±0.05	1	BO_3^{3-}
		calcite	16.6 ±0.5	n.d.	n.d.	2	$BO_2(OH)^{2-}$
		Mg-calcite	16.5 ±0.5	n.d.	n.d.	2	"
		aragonite	18.9 ±0.5	2.8 ±0.1	n.d.	2	"
	natural	biogenic calcite	18.9 ±1	2.8 ±0.3	0.5 ±0.05	1	$BO_2(OH)^{2-}$
			19.3	2.6	0	3	BO_3^{3-}
		biogenic aragonite	16.8	2.5	0	3	$B(OH)_3$
			18.3	2.5	0	3	"
		coral CoC	17.5	2.3	0.2	4	"
tetragonal	synthetic	calcite	0.5 ±1	0.0 ±0.3	-	1	$B(OH)_4^-$
			1.9 ±0.5	n.d.	-	2	"
		calcite ("interstitial")	-0.3 ±0.5				?
		calcite ("interstitial")	-2.4 ±0.5				?
		Mg-calcite	1.2 ±0.5	n.d.	-	2	$B(OH)_4^-$
		aragonite	1.6 ±0.5	0.0 ±0.3	-	1	"
			1.6 ±0.5	n.d.	-	2	"
	natural	biogenic calcite	1.1 ±1	0.0 ±0.3	-	1	$B(OH)_4^-$
			1.67	0.0	-	3	"
		hydrothermal calcite	2.85	0.0		3	?
		biogenic aragonite	1.2 ±0.5	0.0 ±0.3	-	1	$B(OH)_4^-$
			2.54	0.0	-	3	?
			2.0	0.0	-	3	$B(OH)_4^-$
		coral CoC	1.5	0.1	-	4	"

724 *references: [1]Sen et al. (1994), [2]Mavromatis et al. (2015), [3]Klochko et al. (2009), [4]Rollion-Bard et al. (2011)

725

726

727 **Figure captions**

728

729 Figure 1: Theoretical structure of B-bearing calcite and aragonite obtained from first-
730 principles modeling. The H-bond with an oxygen atom of a neighboring carbonate group
731 is indicated by a dotted line. The star in the tetragonal models indicates the Ca atom
732 closest to boron, which has been selected to test the effect of Na^{+} for Ca^{2+} substitution.
733 This atom is located at a distance of 3.09 Å and 3.05 Å from the boron atom in calcite and
734 aragonite, respectively.
735 Red: oxygen, blue: calcium, black: hydrogen, purple: carbon, green: boron.

736

737 Figure 2: Summary of first-principles metadynamic run on aragonite. The fluctuations of
738 SPRINT coordinates (top and middle panel) reflect the geometrical changes affecting the
739 H-bonding pattern of OH groups with O atoms belonging to surrounding carbonate
740 groups. The bottom panel reports the history dependent bias potential which drives the
741 system away from the previously explored configurations (see text). SPRINT
742 coordinates are defined through the product of the principal eigenvalue of the (real
743 valued) adjacency matrix with its corresponding eigenvector. To enforce invariance
744 under permutation of identical atoms, the resulting values are sorted in ascending order
745 within the oxygen and hydrogen subsets, and are shown with a color gradient ranging
746 from the lowest to the highest components.

747

748 Figure 3: Summary of first-principles metadynamic run on calcite. Legend as in Figure 2.

749

750

Figure 4: Theoretical and experimental ^{11}B NMR chemical shifts of trigonal boron. Full symbols: theoretical values from Table 1, open symbols: experimental values from Table 2. The circles correspond to nil or weak η parameters; whereas the squares correspond to high η values indicating in-plane distortion of the trigonal group. The triangles correspond to experimental data for which the η parameter is lacking.

Figure 5: Theoretical and experimental ^{11}B NMR chemical shifts of tetragonal boron. Full symbols: theoretical values from Table 1, open symbols: experimental values from Table 2.

Theoretical structure of B-bearing calcite and aragonite
Click here to download high resolution image

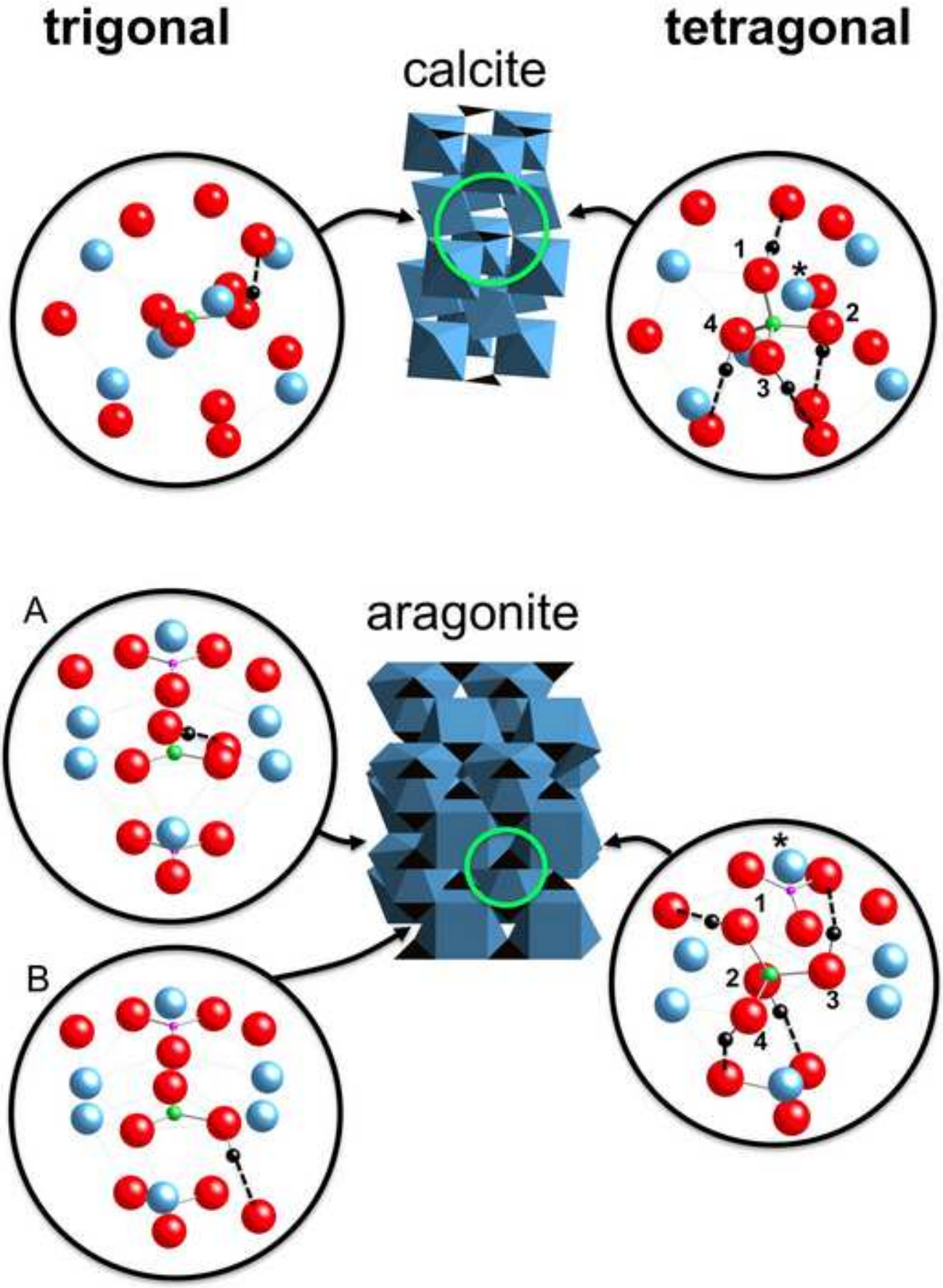

Summary of first-principles metadynamic run on aragonite.
Click here to download high resolution image

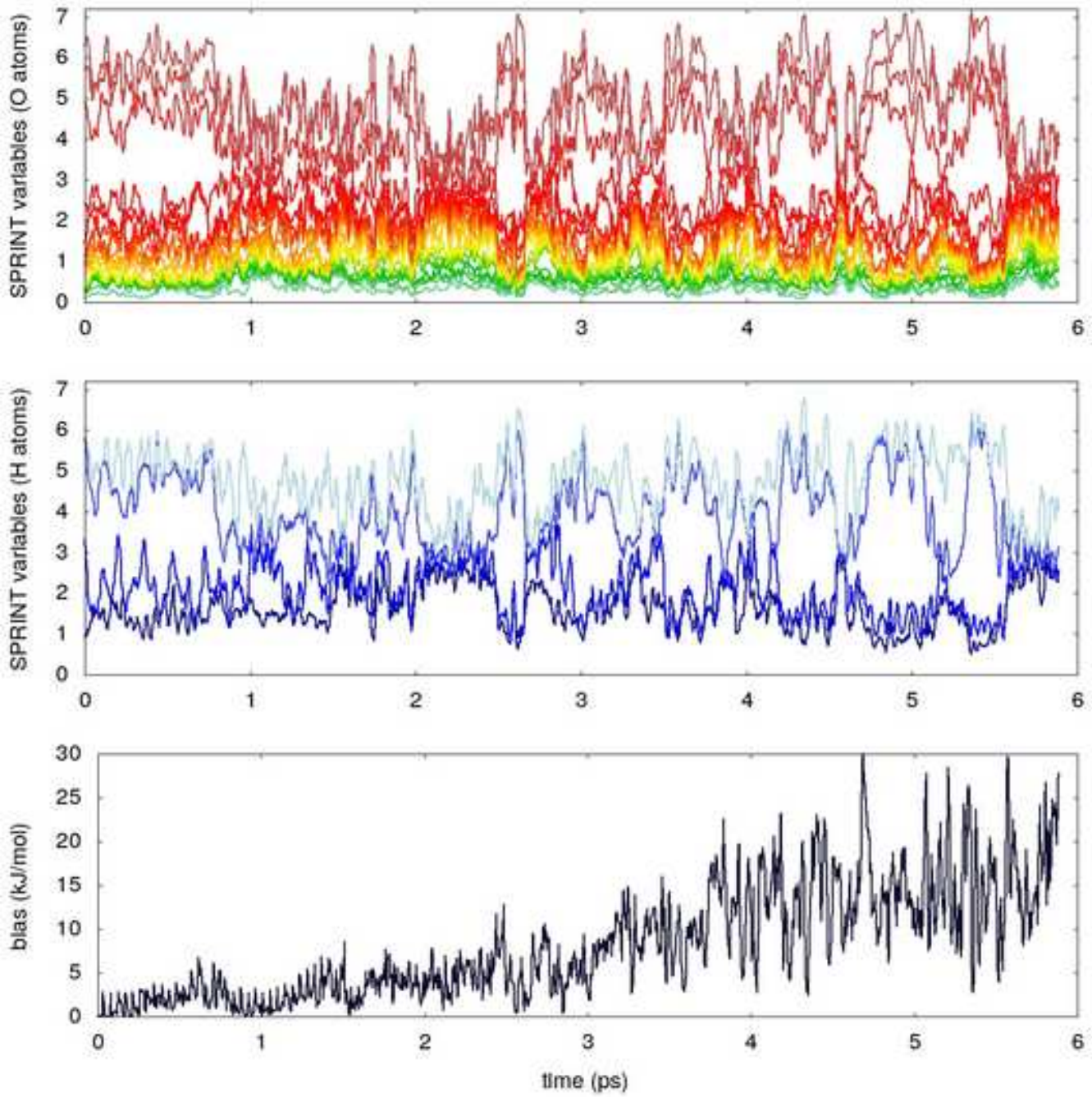

Summary of first-principles metadynamic run on calcite.
Click here to download high resolution image

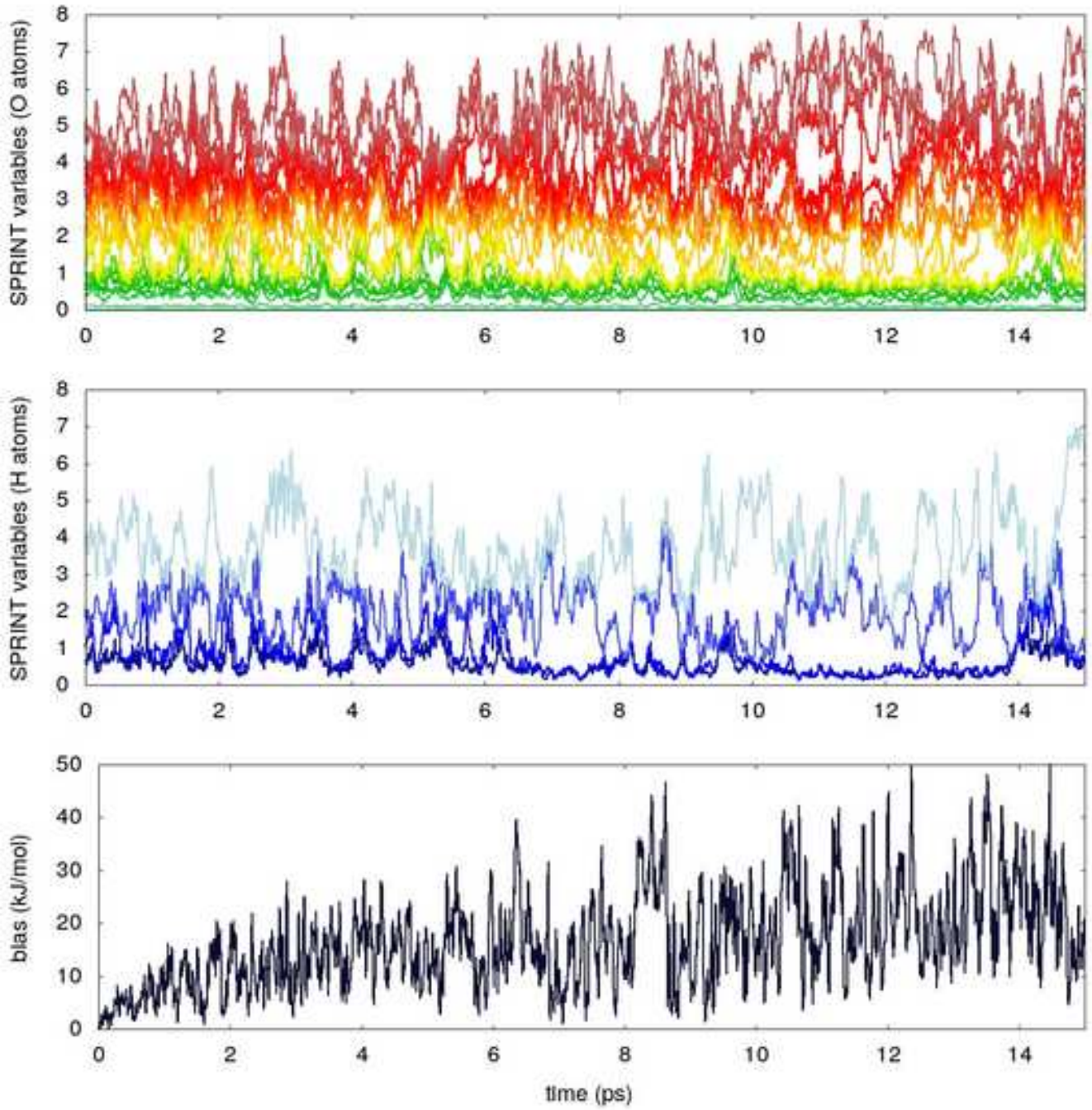

11B NMR chemical shifts of trigonal boron

Click here to download high resolution image

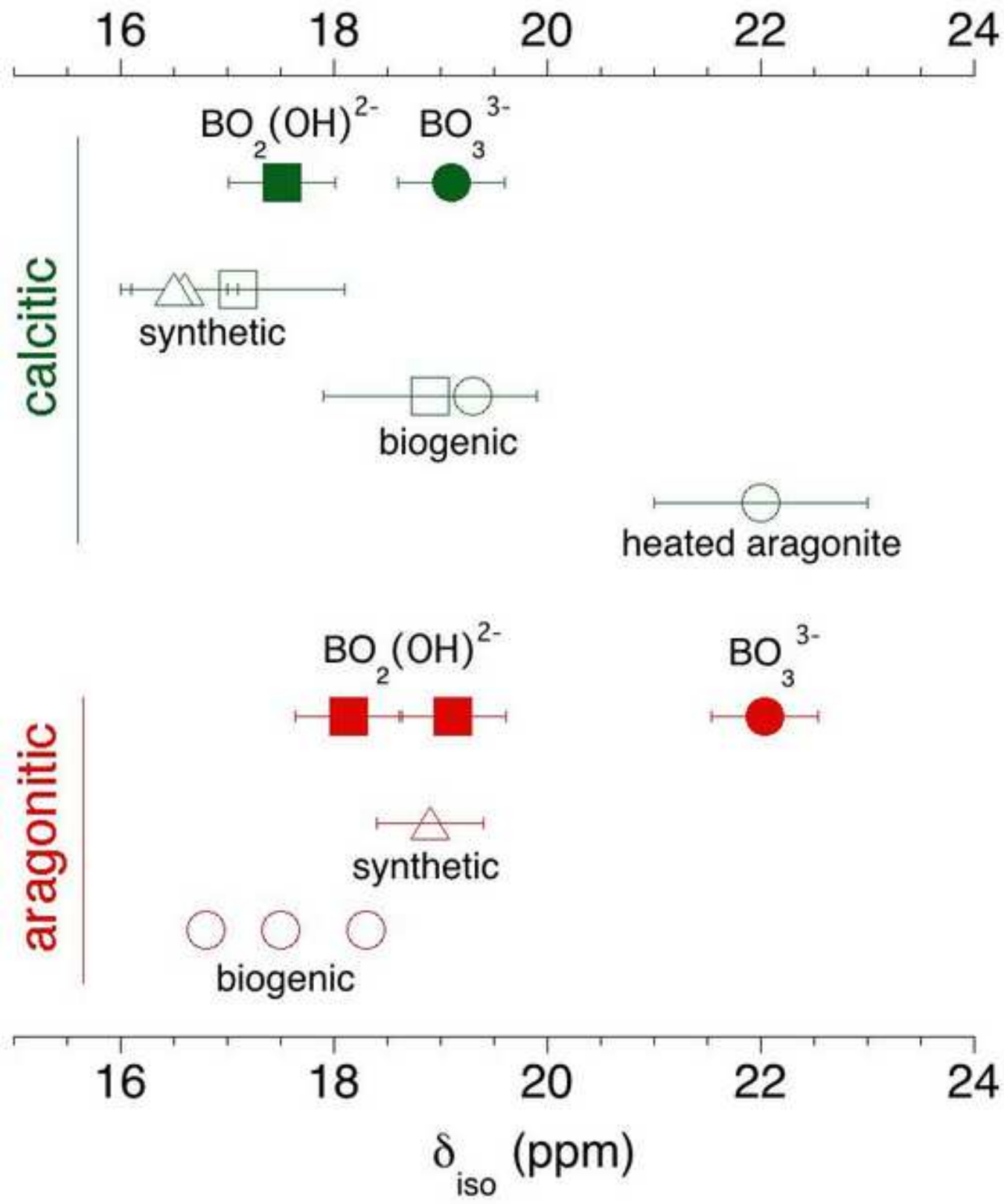

11B NMR chemical shifts of tetragonal boron

Click here to download high resolution image